ADVANCED FUNCTIONAL MATERIALS
www.afm-journal.de

Effect of Trace Solvent on the Morphology of P3HT:PCBM Bulk Heterojunction Solar Cells

*Lilian Chang, Hans W. A. Lademann, Jörg-Bernd Bonekamp, Klaus Meerholz, and Adam J. Moulé**

The performance of bulk-heterojunction (BHJ) solar cells is strongly correlated with the nanoscale structure of the active layer. Various processing techniques have been explored to improve the nanoscale morphology of the BHJ layer, e.g., by varying the casting solvent, thermal annealing, solvent annealing, and solvent additives. This paper highlights the role of residual solvent in the "dried" BHJ layer, and the effect of residual solvents on PCBM diffusion and ultimately the stability of the morphology. We show that solvent is retained within the BHJ film despite prolonged heat treatment, leading to extensive phase separation, as demonstrated by the growth in the size and quantity of PCBM agglomerates. The addition of a small volume fraction of nitrobenzene to the casting solution inhibits the diffusion of PCBM in the dry film, resulting in smaller PCBM agglomerates, and improves the fill factor of the BHJ device to 0.61 without further tempering. The addition of nitrobenzene also increases the P3HT crystalline content, while increasing the onset temperature for melting of P3HT side chains and backbone. The melting temperature for PCBM is also higher with the nitrobenzene additive present.

1. Introduction

Recently, interest in OPVs (organic photovoltaics) has increased because of its potential to deliver low-cost printable PV devices. The photoactive materials can be solution-coated and are compatible with flexible substrates and roll-to-roll fabrication technology, making this technology attractive for industrial scale-up.[1,2] In addition, OPV offers the flexibility of chemical tailoring, expanding opportunities for new materials research. The current certified record power conversion efficiency (PCE) is 8.13%.[3] Most OPV devices consist of a single bulk-heterojunction (BHJ) active layer, in which the electron donor (conjugated polymer) and electron acceptor (fullerene) are deposited from a common solvent. As the solvent dries, the electron donor and electron acceptor phase-separate to form nanoscale interpenetrating networks with charge-separating heterojunctions[4,5] throughout the photoactive layer. The ideal BHJ nano-morphology contains domains that are smaller than ten nanometers in size for efficient exciton dissociation due to the typical exciton diffusion length of less than 10 nm.[6] Recently, OPV research has been dominated by the poly(3-hexylthiophene):[6,6]-phenyl C61-butyric acid methyl ester (P3HT:PCBM) blend. The best P3HT:PCBM blend solar cells deliver PCEs of 4–5%.[7–9]

Despite recent advances, PCEs for OPV still need to be considerably improved for them to be successfully commercialized. Throughout literature, significant advances in PCE are achieved by improvement in morphology.[7,8,10] The challenge in improving PCE is to optimize the interfacial area of the donor/acceptor materials and improve charge mobility within the active layer by increasing mesoscopic order and crystallinity. The efficiency of solar cells based on the P3HT/fullerene system depend strongly on processing conditions[11,12] and can be improved by increasing the crystalline content of P3HT using various methods. BHJ films are usually fabricated by spin-coating. A controlled thermal annealing step after active layer-deposition has been introduced as a way to improve morphology of the BHJ layer and increase the quantum efficiency of the device.[10] An optimal phase-separated morphology for maximum PCE is a non-equilibrium mixture with nanoscale phase separation and connectivity. The morphology of "improved" BHJ layers have been studied using transmission electron microscopy (TEM),[13,14] grazing-angle X-ray diffraction (XRD),[15,16] atomic force microscopy (AFM),[17] and a variety of other techniques.[18,19] All of the morphology studies agree that the P3HT forms ordered crystalline domains upon thermal annealing.

Since molecular order in both the P3HT and PCBM domains is an important factor for high device performance,[15,20–22] researchers have also looked into alternatives to thermal treatment. Solvent annealing has been reported to enhance solar cell performance.[7,23,24] Excess solvent allows the components to remain partially dissolved and diffuse at a higher rate to arrange into a more energetically favorable ordered structure,

L. Chang, Prof. A. J. Moulé
University of California
Davis, 1 Shields Ave
Chemical Engineering and Material Science
Davis, CA 95616, USA
E-mail: amoule@ucdavis.edu
H. W. A. Lademann, Dr. J.-B. Bonekamp, Prof. K. Meerholz
Universität zu Köln
Department Chemie
Luxemburgerstr. 116, 50939 Köln, Germany

DOI: 10.1002/adfm.201002372

thus increasing the crystallinity of the P3HT component.[15,23] The morphological changes that transpire during thermal and solvent treatment of BHJ layers have been detailed in recent review articles.[11,25]

Solvent additives have also been explored as a viable way to improve the morphology of BHJ.[26] Various solvent additives, e.g., alkanedithiols,[27] 1-chloronaphthalene (CN),[28] 1,8-diiodooctane (DIO),[29] and nitrobenzene (NB)[30] have been explored. These additives affect the P3HT-PCBM phase-separation mechanism in BHJ films.[31] Alkanedithiols and DIO are selectively better solvents for the PCBM than for P3HT, which drives the P3HT to self-stack and arrange into ordered domains, while allowing PCBM to remain in solution longer to avoid excessive PCBM aggregation.[29] CN is a good solvent for both the P3HT and the PCBM, and allows a longer time for P3HT chains to self-organize into highly ordered molecular structure for higher hole mobility.[28] NB is a non-solvent for both P3HT and PCBM. The addition of NB to the casting solvent causes the solvent quality for P3HT to gradually decline during spin-coating due to evaporation, consequently increasing aggregation and order within the P3HT domains.[30]

Macroscopic phase separation of PCBM from P3HT:PCBM blends has been observed by several groups.[18,21,32–34] PCBM crystals have been found in both thermally annealed[18,21,32–34] and solvent annealed[35] BHJ active layers. Swinnen et al.[32] noted that the spatial distribution and dimensions of PCBM crystals can be tuned by controlling P3HT:PCBM blend ratios and annealing conditions. Müller and colleagues[33] constructed a non-equilibrium temperature/composition diagram of the P3HT/PCBM binary system from differential scanning calorimetry (DSC) thermograms. Campoy-Quiles et al.[18] proposed a morphology evolution involving vertical and lateral phase separation of P3HT and PCBM, and suggested that crystallization of the P3HT chains occurs first followed by the diffusion of PCBM molecules to nucleation sites where PCBM agglomerations grow. Bull et al.[35] observed formation of mesoscopic PCBM crystallites in solvent annealed BHJ layers and concluded that the formation of large PCBM crystallites does not improve device efficiency. They postulated that higher device performance can be obtained by inhibiting the formation of large PCBM crystallites. There are recent attempts to quantify PCBM diffusion in BHJ films.[34] It is interesting to note that Erb et al.[15] were not able to detect PCBM crystallites using XRD. Due to this conflict of information, we will use "agglomerates" and "aggregates" to describe macroscopic PCBM domains in this article.

BHJ devices have become very popular for OPV devices due to the ease of processing. It is known that some amount of solvent is retained within spin-cast polymer films.[36,37] Although it is the general belief that the annealing step after spin-coating of the BHJ active layer should remove residual solvent in the film, some research has shown that solvent removal from polymeric thin films is not trivial.[38,39] We highlight in this paper the consequence of residual solvent in the P3HT:PCBM BHJ active layer. The main objectives of this research are to examine the role of trace solvent in affecting the morphology and diffusion rate of PCBM in the active layer by monitoring the extent of phase separation. The ultimate goal is to establish an understanding of how device fabrication conditions effects the stability of morphology, so that we can explore methods to increase device lifetime.

2. Results and Discussion

2.1. Diffusion of PCBM

Figure 1 shows a comparison between P3HT:PCBM (1:1) BHJ films that were cast from chlorobenzene (CB) (left) and *ortho*-dichlorobenzene (ODCB) (right). The films were subsequently annealed at 150 °C for increasing times. Reflected optical microscopy (ROM) was used to monitor the degree of phase separation. Microscope images were collected using a CCD camera. Agglomerations were observed in all films that underwent heat treatment at 150 °C while untreated films were featureless at the micrometer scale. The agglomerations were assigned to

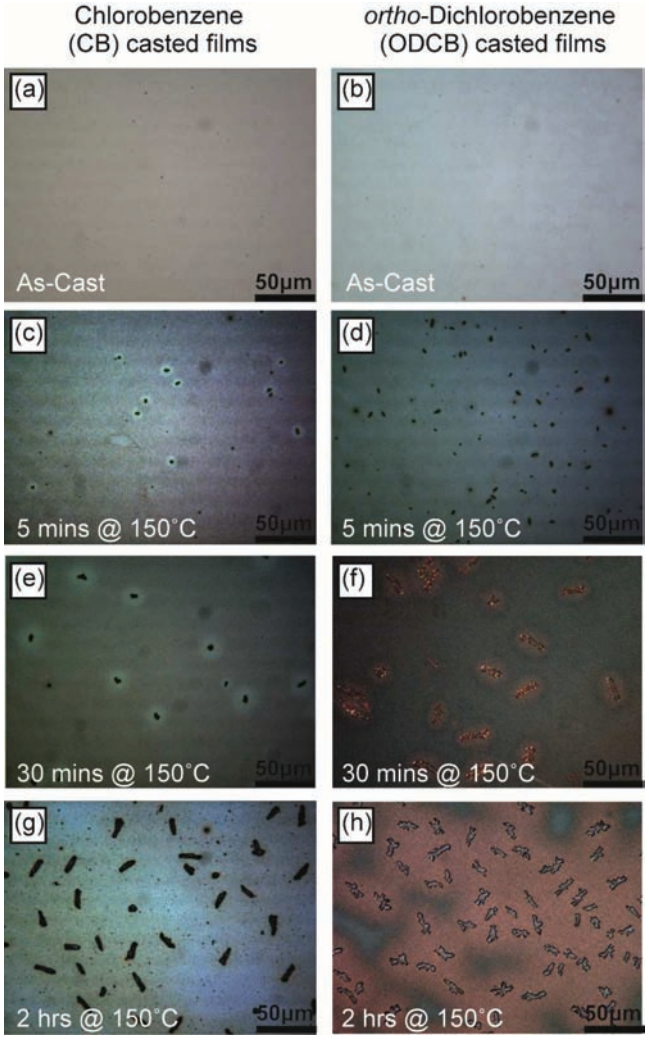

Figure 1. Microscope images of P3HT/PCBM (1:1) films spin-coated from (left) chlorobenzene (CB) and (right) dichlorobenzene (ODCB), a)–b) as-cast, and c)–h) then heat-treated for different durations in a nitrogen glove box.

PCBM-rich domains as previously reported.[18,20,21] The size of PCBM agglomerations increases as the duration of heat treatment increases. This is consistent with Oswald ripening. Ripening is particularly evident in the transition of Figure 1d to Figure 1f. The colored 'halos' around the agglomerations are due to light interference originating from changes in film thickness and are attributed to PCBM-depleted regions.[21] The size of the depletion region increases as the size of the agglomerations increases, suggesting that prolonged heat treatment at 150 °C causes PCBM to diffuse into growing PCBM agglomerates, which acts as a localized sink. This indicates that PCBM has a high mobility within the P3HT matrix at 150 °C. The size and number density of PCBM agglomerations in ODCB-cast samples are greater compared to CB-cast samples after heat treatment, which suggest that the PCBM diffusion rate is higher in layers cast from ODCB. ODCB has a higher boiling point (bp 180 °C) compared to CB (bp 131 °C). A higher diffusion rate is probably the result of a larger amount of excess solvent remaining within the film, causing the film to be softer, and increasing the diffusion rate of PCBM in the heated film.

The idea that excess solvent within the active layer increases the diffusion rate of PCBM prompted the use of a chemical test to investigate whether casting solvent remains trapped in a BHJ layer before and after heat treatment. Gas chromatography–mass spectrometry (GCMS) was performed on re-dissolved BHJ films. **Figure 2** shows GCMS traces from ODCB-cast BHJ films that were re-dissolved in chloroform. Figure 2a shows that ODCB peaks were present after the ODCB-cast films were annealed at 150 °C for 1, 5, and 10 min in an N_2 glove box. ODCB was also detected in BHJ films that were subjected to vacuum for up to 21 h (Supporting Information, Figure S1). However, solvent peaks were not detected in ODCB-cast films that were annealed in a fume hood with face velocity ca. 180 feet per minute, as shown in Figure 2b. The GCMS experiment confirms that solvent molecules are trapped within the BHJ films in fairly high concentrations for films that were heat-treated inside the N_2 glove box. This is also observed with CB-cast films (Supporting Information, Figure S2). Note that the glove box used is equipped with a molecular sieve solvent trap and is under a continuous gas flow; this test was performed immediately after regenerating the O_2 catalyst and solvent trap, and after 48 h of no solvent use in the glovebox. GCMS cannot be used to determine the absolute concentration of solvent in the BHJ film because the re-dissolution of the film is a manual process that results in differing ratios of film content to chloroform.

To further investigate the effects of trace solvents in the formation of PCBM agglomerates on the surface of the BHJ layer, a series of ODCB-prepared P3HT:PCBM (1:1) BHJ samples were prepared on glass. The BHJ samples were then annealed at 150 °C with differing solvent environments and ROM was used to examine the degree of phase separation. **Figure 3** compares ROM images of an ODCB BHJ layer as-cast (a), annealed at 150 °C for 30 min under normal glove box environment (b), annealed under ODCB-saturated environment (c), and annealed under forced convection (d), where a recirculation pump is used to increase the exchange rate of the nitrogen environment in the immediate vicinity of the sample surface. Figure 3 clearly shows that increasing the vapor pressure of

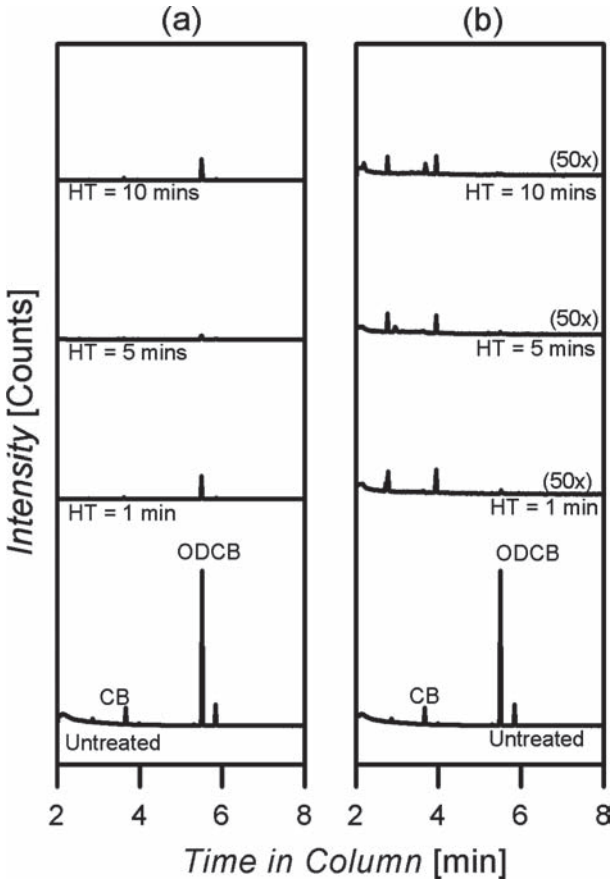

Figure 2. Comparison of GCMS trace of ODCB-cast films, a) before and after heat treatment (HT) in a nitrogen glove box, and b) before and after heat treatment in a fume hood (in air). Traces are shifted vertically for clarity.

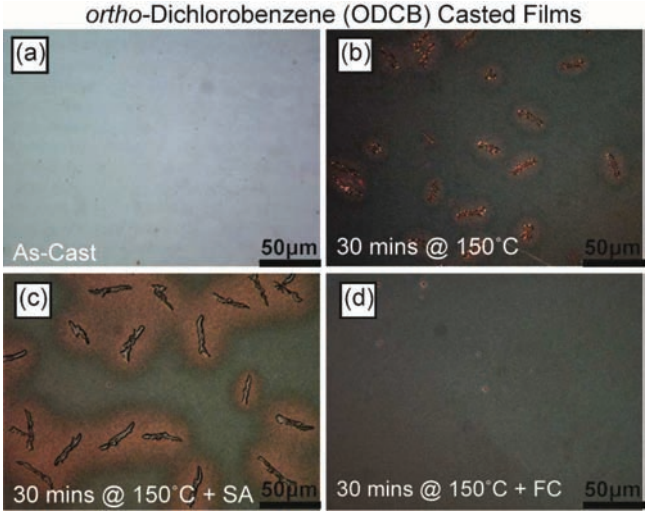

Figure 3. Microscope images of P3HT/PCBM (1:1) films spin-coated from ODCB, a) as-cast, b) after annealing at 150 °C for 30 min, c) after annealing at 150 °C in an ODCB-saturated solvent atmosphere (SA) for 30 min, and d) after annealing at 150 °C for 30 min under forced convection flow (FC).

solvent in the local environment increases the size of PCBM agglomerations. PCBM agglomerations were largest when the BHJ film was annealed under saturated vapor pressure conditions (Figure 3c) and these results are consistent with our assertion that trapped solvents promote higher rate of PCBM diffusion into localized sinks. When solvent is driven out of the film using forced convection, the film is almost featureless as shown in Figure 3d. This suggests that while solvent annealing is shown to benefit solar cell performance comparable to heat-treated devices,[23] the morphology of solvent-annealed devices may not be as stable, since phase separation will continue to take place at a faster rate due to higher amounts of trapped solvent. The results in Figure 3 coupled with the GCMS results in Figure 2 highlight the role of vapor pressure in solvent entrapment within the BHJ layer.

Figure 4 shows a cartoon that explains the effect of the local environment – moving air flow (left) versus nitrogen glove box (right) – on solvent entrapment within the BHJ layer during heat treatment. The vapor pressure for ODCB in the fume hood and under forced convection nitrogen flow is essentially zero, so ODCB is readily removed from the film when the film is subjected to heat treatment. Although the vapor pressure of ODCB in a nitrogen glove box with continuous flow and a molecular sieve solvent trap is considerably lower than the saturated vapor pressure (1.2 Torr at 20 °C), it is still above zero, especially in the direct local environment where the BHJ films were deposited and tempered. Hence, when heat is applied, ODCB slowly evaporates from the BHJ film until an equilibrium is achieved with the vapor phase; some solvent remains within the film.

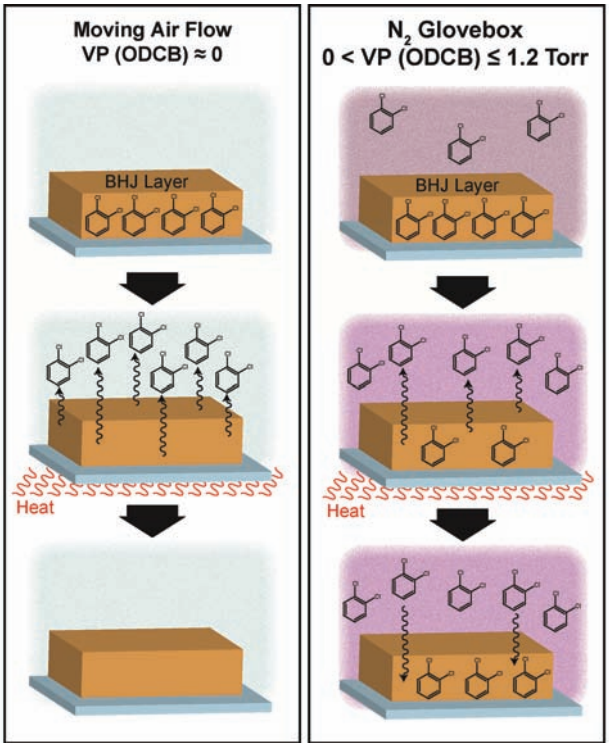

Figure 4. Schematic illustrating the effect of the environment (moving air versus nitrogen glove box) on solvent entrapment within the BHJ layer.

When heat is removed from the film, a new equilibrium is achieved where ODCB diffuses back into the film. We proved this assertion by spin-casting both CB and ODCB films using the same spin-coater in an N_2 glove box. In the GCMS traces, ODCB was detected in the CB-cast film (Supporting Information, Figure S2b). This shows that solvent is reabsorbed into the films. The local solvent environment around the hot plate or spin-coater in the nitrogen glove box prevents evaporation of excess solvent trapped within the BHJ layer. Our results clearly show that as long as traces of solvents remain within the layer, PCBM domains will continue to grow rapidly as the BHJ layer is subjected to heat treatment. This phenomenon is probably the reason why BHJ devices fabricated in different labs have different morphologies and hence different performances.

We showed that agglomerations of PCBM-rich domains grow in size and quantity with increasing heat treatment time. In order to correlate the observed phase separation to device performance, the effect of PCBM agglomerations on photocurrent was investigated using laser beam induced current (LBIC) mapping. LBIC involves focusing a 405 nm diode laser to a spot size of 50 μm^2 and then scanning over the film using positioning mirrors. The resulting photocurrent at each location is recorded, resulting in a map of the local photocurrent under short-circuit conditions. **Figure 5**b shows a LBIC map of P3HT:PCBM film cast from ODCB and annealed at 150 °C for 2 h. This image was recorded with a Ca electrode deposited on top of the film. In order to probe if the colored regions corresponds to any features on the film, the Ca electrode was removed using water[40] and then inspected under an optical microscope as shown in Figure 5a. Comparison of the microscope image and LBIC map shows that regions of high photocurrents (blue and dark blue regions) are regions that are free of PCBM agglomerates while regions of low photocurrents (green) are regions where PCBM agglomerates are present. The presence of large PCBM agglomerations reduces the local photovoltaic efficiency of the device even for excitation at 405 nm, which should favor absorption into PCBM (Supporting Information, Figure S3).

Another interesting observation from Figure 5a is that PCBM agglomerations within the footprint of the Ca electrode are much larger than the agglomerations outside the footprint. This may be due to surface energy effects.[41] However, we believe that the Ca electrode hinders solvent from leaving

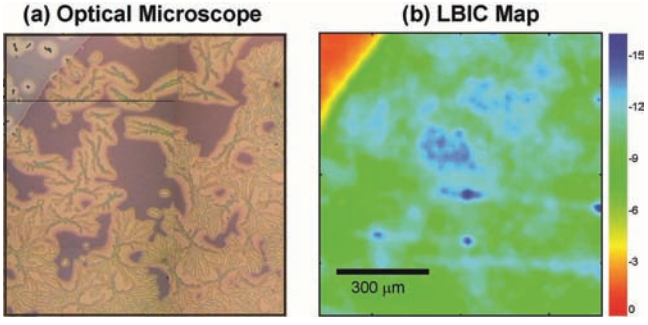

Figure 5. a) Microscope and b) LBIC images of an ODCB cast device with a thickness of 150 nm. LBIC images were collected with a pure Ca electrode. This electrode was later removed for optical microscopy.

the BHJ layer, effectively trapping the solvent within the film, and allowing PCBM to diffuse at a high rate to form larger agglomerates.

2.2. Hindering PCBM Diffusion

LBIC results suggest that large mesoscopic-scale PCBM agglomerates may be detrimental to device performance. Our studies of PCBM diffusion in a glove box environment with filtered atmosphere showed that solvent removal from the film can be very difficult, and this difficulty can only increase as the device area increases. In order to address morphological stability for scaled-up OPV printing, we investigate whether the size and density of PCBM agglomerates can be reduced via the addition of a chemical additive.

We have shown that some amount of the casting solvent remains within the BHJ film even after heat treatment, and that the presence of trace solvent can accelerate phase separation between the polymer and fullerene component during heat treatment and adversely affect device performance. The thermal stability of a BHJ layer is important considering that the device temperature on a rooftop can reach 80°C and device lifetime of more than 5 years is necessary. We speculate that solvent additives will have a greater effect on morphology than host solvents due to their higher boiling point (bp). We investigated the effects of various additives on the stability of the BHJ morphology under heat stress. BHJ films were prepared using pure CB, with 4% NB additive, with 4% DIO additive, and with 4% CN additive. These processing additives all have higher bp compared to CB. Based on the GCMS results above, we expect that the processing additives will remain in the film during and after heat treatment at 150 °C.

The degree of phase separation after heat treatment at 150 °C for 30 min was monitored using ROM, and the results are shown in **Figure 6**. After 30 min of heat treatment, BHJ films spin-coated from 4% NB/CB, shown in Figure 6b, has the least amount of PCBM agglomeration on the mesoscopic scale compared to a purely CB-cast film (Figure 6a), and BHJ films with DIO and CN additives (Figure 6c and Figure 6d). BHJ film spin-coated from 4% CN/CB, as shown in Figure 6d, exhibits the highest extent of phase-separation with the largest agglomerates, while films spin-coated from 4% DIO/CB (Figure 6c) also have larger PCBM agglomeration than the pure CB-cast film. From Figure 6, the extent of phase separation in the heat-treated BHJ film can be summarized in the following order, from the most phase-separated to the least phase-separated, 4% CN/CB > 4% DIO/CB > CB > 4% NB/CB. This result is consistent with previous explanations of the phase-separation mechanism. CN is a good solvent for both P3HT and PCBM.[28] CN allows both components to remain in solution for a longer period of time, increasing the mobility of both phases within the BHJ layer and accelerating phase separation due to their high solubility in the solvent and poor solubility in one another. DIO preferentially dissolves PCBM and is a poor solvent for P3HT.[29] With DIO present, P3HT is driven to self-stack into structured domains while PCBM is still mobile within the BHJ layer, allowing PCBM to diffuse into localized PCBM sinks and agglomerate. The extent of phase separation is reduced for DIO than for the case of CN, possibly due to the formation of P3HT ordered domains which impedes PCBM diffusion. NB is a poor solvent for both P3HT and PCBM.[30] When NB is used as the additive, P3HT self-assembles into aligned structures, forming an interpenetrated network. PCBM diffusion is inhibited by the aggregated P3HT network and its limited solubility in NB. The NB/CB film appears to be more textured than the CB film as was previously reported.[30]

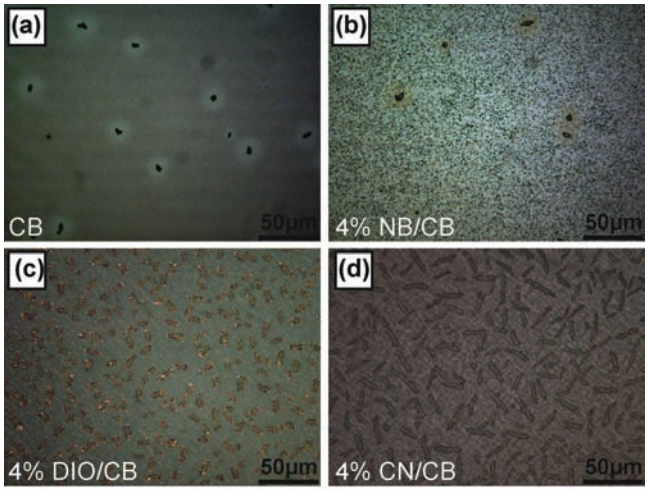

Figure 6. Microscope images of P3HT/PCBM (1:1) films spin-coated from a) CB, b) 4% NB added to CB, c) 4% DIO added to CB, and d) 4% CN added to CB. Films were heat-treated in a glove box for 30 min at 150 °C.

The addition of a small volume fraction of NB into the BHJ casting solution appears to hinder PCBM diffusion and inhibit the growth of PCBM agglomerations. In order to investigate the effect of NB additive to the morphology of the BHJ film, we monitor the change in crystallinity of P3HT. Previous studies have shown that the aggregated content of P3HT can be increased up to the equivalent of a pure slow-cooled film by addition of NB.[30] Changes in crystallinity of P3HT with respect to temperature can be examined by monitoring the change in absorbance for the vibronic peak at ca. 610 nm. This peak is assigned to an interchain-delocalized excitation[42] and its intensity has been linked to the degree of P3HT crystallinity.[22] UV–vis spectra of films were taken in reflection geometry. These measurements were performed on BHJ films that were first heated for 5 min at 150 °C for CB-cast film and 180 °C for 4% NB/CB cast film, then cooled to room temperature. Absorption spectra were measured at intervals of 10°C during cooling to room temperature. 180°C was the upper heating limit for the experiment due to worries of deformation to the sample holder. **Figure 7**a and b show the evolution of absorption spectra with respect to temperature for BHJ layers cast from CB and 4% NB/CB respectively. There are differences in the total absorption of the two films due to slight differences in film thickness and especially since the NB-added layer is rougher compared to the pure CB-film. The height of the peaks at ca. 610 nm with respect to temperature is normalized to a 0 to 1 scale using $A_\theta' = (A_\theta - A_{min})\ (A_{max} - A_{min})^{-1}$, where A is the measured absorbance at ca. 610 nm at temperature θ, while A_{min} is the minimum measured absorbance at ca. 610 nm and A_{max} is the maximum

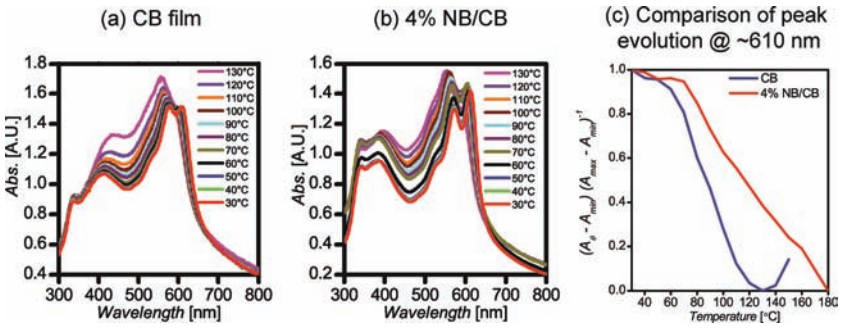

Figure 7. Absorption spectra in reflection geometry collected at different temperature for a) a CB-cast film, and b) a 4% NB/CB-cast film. c) A comparison of the change in absorption intensity of the 610 nm shoulder (normalized to [0,1] scale) from the spectra collected in (a) and (b).

measured absorbance of the 610 nm peak. The intensity of the peak at ca. 610 nm should be at its lowest at high temperatures since P3HT has the highest disorder while the highest degree of P3HT ordering should occur at the lowest temperature achievable by the experimental set-up. By comparing the change in the normalized intensity of the peak at ca. 610 nm as shown in Figure 7c, it is observed that for the CB–BHJ film, the intensity of the peak remains almost unchanged during cooling from 140 °C to 120 °C. This is the state where the film has the highest disorder and the lowest P3HT crystalline content. The intensity of the peak starts to grow as the film is cooled below 120 °C, indicating the onset of P3HT ordering. As the film is cooled from 120 °C to ca. 50 °C, the peak grows linearly with respect to cooling temperature, suggesting increasing P3HT crystalline content as the BHJ sample is cooled. The intensity of the peak no longer changes linearly with respect to temperature at temperatures below 50 °C, suggesting that P3HT has achieved almost maximum ordering. In the case of the 4% NB/CB–BHJ film, the growth of the crystalline peak at ca. 610 nm starts immediately after heat treatment, even when heat treatment was carried out at 180 °C. This suggests that P3HT crystalline domains are forming even at high temperatures of above 150 °C. The 610 nm peak grows linearly as the sample is cooled from 180 °C to ca. 70 °C, where the peak intensity remains almost unchanged, implying maximum ordering in the P3HT phase. P3HT domains in the NB-added sample achieve maximum ordering at a higher temperature (ca. 20 °C higher) compared to a pure-CB sample. The reflectivity results show that P3HT stacks in ordered domains at higher temperatures when NB is added to the CB-casting solvent.

Figure 8 shows DSC heat flow (HF) heating curves comparing CB-cast and 4% NB/CB-cast BHJ films. The heating curves were collected after an isothermal step at 150 °C for 30 min to emulate the heat treatment step. The phase transition observed at approximately 50 °C in the CB-cast film has been attributed to the melting of the P3HT side chain.[43] This phase transition is observed at 150 °C for the 4% NB/CB film. The addition of NB to the casting solvent appears to alter the crystallization behavior of the P3HT side chains. The heating curves in Figure 8 show that the onset of melting for the P3HT conjugated backbone occurs at around 150 °C for a CB-cast sample, while the onset of melting for a 4% NB-added sample occurs at ca. 190 °C. This means that the stacked P3HT backbone begins to lose order at a lower temperature in a pure-CB cast BHJ film, compared to when NB is used as an additive. This also suggest that the P3HT crystals in the NB/CB BHJ film are more thermally stable compared to P3HT crystals in a pure CB BHJ film, which is in agreement with the results in Figure 7. The melting point of the bulk crystalline P3HT backbone is the same for both films (ca. 208 °C). The melting point of PCBM however is approximately 13 °C higher for a 4% NB/CB BHJ film compared to a pure CB BHJ film. Heating curves for pristine PCBM powder after an isothermal step at 150 °C for 30 min shows two melting temperatures (Supporting Information, Figure S4). This is probably due to the PCBM adopting two different crystal structures. Rispen et al.[44] have shown that PCBM crystal can adopt either a monoclinic or triclinic crystal structure when crystallized from different solvents. The increase in PCBM melting temperature when NB is added to the BHJ film indicates the formation of a more thermally stable PCBM crystal structure compared to PCBM crystals found in a pure CB-cast film. Also the broader endothermic PCBM melting valley for the CB BHJ film may reflect a distribution of crystal structures.

Figure 9 compares the *I–V* performance of CB-cast and 4% CB/NB-cast devices for increasing heat treatment times. Both types of devices have an active layer thickness of ca. 80 nm. The data presented in Figure 9 were averaged over 8 to 10 devices and collected with 120 mW cm^{-2} (1.2 SUN) of simulated solar illumination. Reported values were not corrected for spectral mismatch. The as-cast CB devices have an average short circuit current (J_{sc}) of 3.37 mA cm^{-2} and a fill factor (FF) of

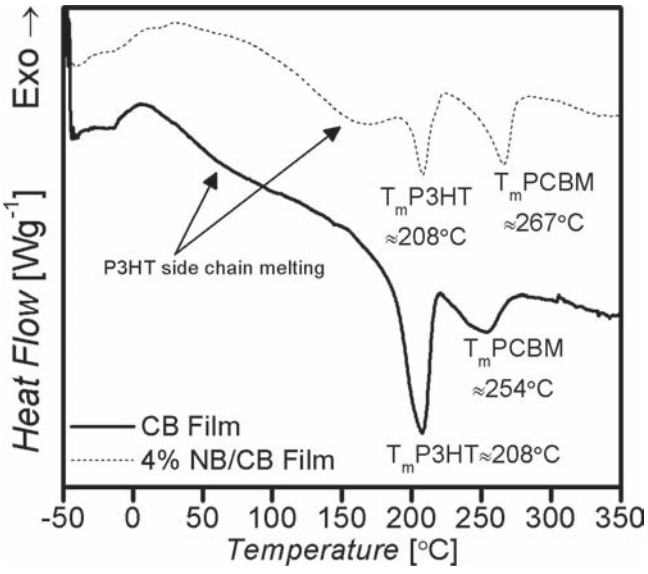

Figure 8. DSC HF heating curves for CB-cast film (solid line) and 4% NB/CB film (dotted line) after an isothermal step at 150 °C for 30 min. Curves are shifted vertically for clarity.

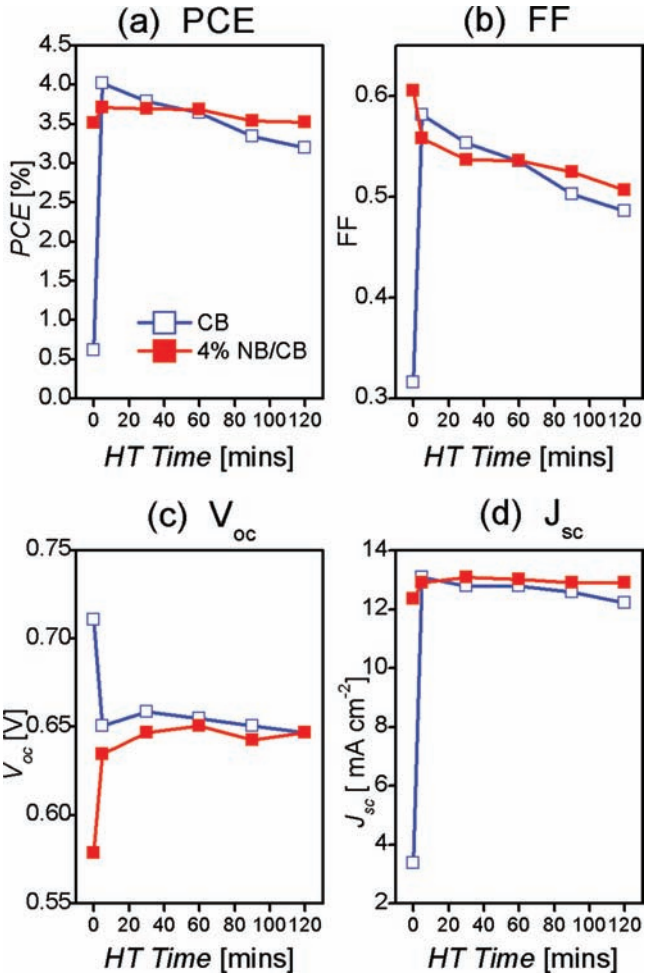

Figure 9. Influence of the duration of heat treatment (HT) at 150 °C on a) power conversion efficiency (PCE), b) fill factor (FF), c) open-circuit voltage (V_{oc}), and d) short-circuit current density (J_{sc}) for CB-cast device (blue, open symbols) and 4% NB/CB-cast devices (red, filled symbols).

0.32. Upon annealing at 150 °C for 5 min, the J_{sc} increased to 13.08 mA cm^{-2} and the FF improves to 0.58, causing the efficiency of the CB-cast devices to increase from 0.61% to 4.02% post annealing. The improved performance with heat treatment have been previously reported.[10] The open circuit voltage (V_{oc}) was found to decrease after annealing, from 0.71V to 0.65V. This decrease in V_{oc} after annealing has been observed for CB-cast devices.[9,45] Although the initial annealing is shown to benefit the performance of the device due to improved order in both the donor and acceptor domains, annealing the CB-cast devices for a longer duration resulted in a decline in power conversion efficiency (PCE) (Figure 9a), mostly due to the decline FF (Figure 9b) and J_{sc} (Figure 9d). The PCE decreased from 4.02% after 5 min of heat treatment to 3.2% after 120 min of heat treatment, due to FF decreasing from 0.58 to 0.48, and J_{sc} dropping from 13.08 mA cm^{-2} to 12.21 mA cm^{-2}. The V_{oc} hovers around 0.65V for all heat-treated CB-devices (Figure 9c). It interesting to note that two of the CB-devices suffered catastrophic failure after heat treatment for 90 min and were no longer included in the averaging of the data thereafter. For the 4% NB/CB-cast devices, the unheated devices have a FF of 0.61, with J_{sc} of 12.4 mA cm^{-2}, and V_{oc} of 0.58 *V*. The efficiency is 3.52%. The FF of an as-cast device with a small volume fraction of NB additive is better than the annealed devices cast from pure CB. After 5 min of annealing at 150°C, the 4% NB/CB devices show higher V_{oc} (0.63 V) while the FF decreases slightly to 0.56. The increase in V_{oc} improved the efficiency of the annealed 4% NB/CB device slightly to 3.72%. As the duration of heat treatment increases, the PCE for 4% NB/CB devices show a slight decline from 3.72%, after 5 min of heat treatment, to 3.52%, after 120 min of heat treatment (Figure 9a). This is largely due to a slight decline in FF from 0.56 (5 min heat treatment) to 0.51 (120 min heat treatment).

Comparing the device performance of devices cast from CB and devices cast with NB additive corroborates the LBIC result, which showed that the formation of large PCBM agglomerates lead to deterioration of device efficiency. The formation of larger agglomerates as the duration of heat treatment increases in the presence of trace CB within the BHJ active layer resulted in a decline in FF, J_{sc} and ultimately a decline in the PCE of the CB devices. It also caused some devices to fail catastrophically. The addition of NB was shown to suppress the formation of PCBM agglomerates. The performance of NB-added devices were more stable showing minimal decline in efficiency even after 2 h of heat treatment at 150 °C.

3. Conclusions

We have shown that the choice of casting solvent has a significant effect on the thermal stability of the morphology of P3HT:PCBM BHJ layers. Even after the solvent is assumed to have evaporated, the active layer has a high affinity towards solvent molecules and can still trap solvent molecules from its immediate environment. Optical microscopy showed the formation of PCBM agglomerations in all heat-treated BHJ layers from both CB and ODCB. We observed that heat treatment of BHJ films cast from ODCB resulted in larger PCBM agglomerations. Since ODCB has a higher boiling point compared to CB, it is not readily evaporated and a larger amount of solvent remains trapped within the BHJ layer. The presence of trapped solvent in the BHJ layer increases the diffusive mobility of PCBM within the polymer matrix, and promotes the growth of larger PCBM agglomerates, increasing the degree of phase separation. Using GCMS, ODCB was detected in the re-dissolved active layer after heat treatment for 10 min at 150 °C. We show that the solvent is removed for an identical annealing time if high convective air flow is introduced. This suggests that while the casting solvent is important, equally important is the solvent environment during heat treatment of the BHJ layer. The morphology can be strongly affected by simply varying the local solvent atmosphere where samples are undergoing heat treatment. Since the morphology of the BHJ layer is highly sensitive to the solvent environment, this can explain the variations in results obtained from different laboratories and even day to day variations within the same glove box. LBIC mapping suggest that large PCBM agglomerates reduces the local photovoltaic efficiency of the device. We highlight that solvent removal from BHJ layers is not a trivial matter and should be

given due consideration during solar cell fabrication, given the effect it has on long term stability of the device morphology.

Several solvent additives were tested to determine if their use increases or decreases the diffusion rate of PCBM and thereby increases or decreases the stable lifetime of the BHJ layer morphology. The use of NB as a chemical additive suppressed the formation of PCBM agglomerates while the other additives tested such as DIO and CN promotes PCBM agglomeration. Absorbance measurements indicate that P3HT remains ordered at higher temperatures when NB is added to the BHJ layer. This observation was confirmed with DSC, where the onset of melting for P3HT side chains and conjugated backbone both occur at higher temperatures with the addition of NB. As-cast devices made with 4% NB added to the CB-casting solution show comparable performance to annealed devices cast purely from CB. The 4% NB/CB devices were also shown to be more thermally stable compared to the CB-cast devices. This is probably due to the suppression of PCBM agglomerations with NB additive, making the BHJ layer more morphologically stable. These results collectively suggest that non-solvent additives should be further investigated to increase the morphological stability of BHJ films.

4. Experimental Section

All the BHJ layers in this work were prepared on either commercially available indium–tin oxide (ITO) coated glass with layer thickness ca. 140 nm and 15 Ω sheet resistances or on glass microscope slides. Substrates were cleaned using chloroform followed by acetone, Mucasol detergent, and de-ionized water in an ultrasonic bath. The ITO substrates were then washed in a spin–rinse–dryer (SRD) system before being exposed to UV–ozone for 30 min. BHJ layers used for ROM (Nikon Labophot-2), GCMS (Varian 3900-Saturn 2100T GCMS), and DSC (Mettler Toledo) were approximately 200 nm thick. Samples for GCMS studies were prepared by re-dissolving the BHJ layers in chloroform. Samples for DSC studies were prepared by delaminating the BHJ layers of interest from the glass substrate and weighing it into an aluminum crucible. Heating curves were collected from –50 °C to 350 °C, at a rate of 20 °C min^{-1}, after an isothermal step at 150 °C for 30 min. Samples used for UV–vis–NIR spectroscopy (Perkin Elmer Lambda 750) studies were approximately 80 nm thick while samples used for LBIC mapping (in-house assembled equipment) were approximately 150 nm thick. Layer thickness was controlled by changing both concentration of the casting solution and spinning speed. Sample thickness was determined using a Dektak surface profiler that was calibrated to a Si-SiO_2 ellipsometry standard.

For device fabrication, the ITO was spin-coated with 40 nm of PEDOT:PSS (Baytron P Al 4083, HC Starck). The PEDOT:PSS coated samples were then heat-treated at 110 °C for 3 min and then moved into a nitrogen glove box for the remainder of the device fabrication and measurement. The CB and ODCB polymer and fullerene solutions were stirred at 60 °C overnight before spin-coating to ensure that the polymer and fullerene has been completely dissolved. The active layer of the solar cells were spin-coated from a 1:1 mixture of P3HT (Aldrich, reported regioregularity ≥ 90%) and PCBM (Nano-C). After spin-coating of the active layer, the samples were moved to a high vacuum chamber (ca. 10^{-6} mbar), where an electrode of 5 nm Ca and 150 nm Ag were vapor deposited through a mask leaving six solar cells with an active area of 0.1690 cm^2. After metal deposition, the samples were either directly measured or annealed for 5 min at 150 °C in an N_2 glove box.

The *I–V* curves of the samples were measured using a Keithley 2420 source measurement unit in an N_2 glove box. AM 1.5 illumination at 120 mW cm^{-2} (1.2 SUN) was provided by a solar simulator (Radiant Source Technology). All reported values are not corrected for spectral mismatch.

Supporting Information

Supporting information is available from the Wiley Online Library or from the author

Acknowledgements

This work was supported by the US Department of Energy EERE Solar America Initiative under Contract No. DE-FG36–08GO18018, the National Science Foundation Energy for Sustainability program, Award No. 0933435, and the German Ministry of Education and Science (BMBF, NanoPolySol project).

Received: November 10, 2010
Published online: March 4, 2011

[1] F. C. Krebs, *Polymer Photovoltaics: A Practical Approach*, SPIE, Bellingham **2008**.
[2] A. J. Moulé, *Curr. Opin. Solid State Mater. Sci.* **2010**, *14*, 123.
[3] Solarmer Energy, Inc. (July 27, **2010**) "Solarmer Energy, Inc. Breaks Psychological Barrier with 8.13% OPV Efficiency". Press release. Retrieved from http://www.businesswire.com/news/home/20100727005484/en/Solarmer-Energy-Breaks-Psychological-Barrier-8.13-OPV (last accessed September 2010).
[4] C. W. Tang, *Appl. Phys. Lett.* **1986**, *48*, 183.
[5] G. Yu, A. J. Heeger, *J. Appl. Phys.* **1995**, *78*, 4510.
[6] D. E. Markov, E. Amsterdam, P. W. M. Blom, A. B. Sieval, J. C. Hummelen, *J. Phys. Chem. A* **2005**, *109*, 5266.
[7] G. Li, V. Shrotriya, J. Huang, Y. Yao, T. Moriarty, K. Emery, Y. Yang, *Nat. Mater.* **2005**, *4*, 864.
[8] W. Ma, C. Yang, X. Gong, K. Lee, A. J. Heeger, *Adv. Funct. Mater.* **2005**, *15*, 1617.
[9] M. Reyes-Reyes, K. Kim, D. L. Carroll, *Appl. Phys. Lett.* **2005**, *87*, 083506.
[10] F. Padinger, R. S. Rittberger, N. S. Sariciftci, *Adv. Funct. Mater.* **2003**, *13*, 85.
[11] H. Hoppe, N. S. Sariciftci, *J. Mater. Chem.* **2006**, *16*, 45.
[12] X. Yang, J. Loos, *Macromolecules* **2007**, *40*, 1353.
[13] X. N. Yang, J. Loos, S. C. Veenstra, W. J. H. Verhees, M. M. Wienk, J. M. Kroon, M. A. J. Michels, R. A. J. Janssen, *Nano Lett.* **2005**, *5*, 579.
[14] S. S. van Bavel, M. Barenklau, G. de With, H. Hoppe, J. Loos, *Adv. Funct. Mater.* **2010**, *20*, 1458.
[15] T. Erb, U. Zhokhavets, G. Gobsch, S. Raleva, B. Stuhn, P. Schilinsky, C. Waldauf, C. J. Brabec, *Adv. Funct. Mater.* **2005**, *15*, 1193.
[16] P. Vanlaeke, G. Vanhoyland, T. Aernouts, D. Cheyns, C. Deibel, J. Manca, P. Heremans, J. Poortmans, *Thin Solid Films* **2006**, *511*, 358.
[17] R. J. Kline, M. D. McGehee, E. N. Kadnikova, J. S. Liu, J. M. J. Frechet, M. F. Toney, *Macromolecules* **2005**, *38*, 3312.
[18] M. Campoy-Quiles, T. Ferenczi, T. Agostinelli, P. G. Etchegoin, Y. Kim, T. D. Anthopoulos, P. N. Stavrinou, D. D. C. Bradley, J. Nelson, *Nat. Mater.* **2008**, *7*, 158.
[19] V. D. Mihailetchi, H. X. Xie, B. de Boer, L. M. Popescu, J. C. Hummelen, P. W. M. Blom, L. J. A. Koster, *Appl. Phys. Lett.* **2006**, *89*, 012107.
[20] D. Chirvase, J. Parisi, J. C. Hummelen, V. Dyakonov, *Nanotechnology* **2004**, *15*, 1317.
[21] T. J. Savenije, J. E. Kroeze, X. N. Yang, J. Loos, *Adv. Funct. Mater.* **2005**, *15*, 1260.

[22] U. Zhokhavets, T. Erb, G. Gobsch, M. Al-Ibrahim, O. Ambacher, *Chem. Phys. Lett.* **2006**, *418*, 347.
[23] G. Li, Y. Yao, H. Yang, V. Shrotriya, G. Yang, Y. Yang, *Adv. Funct. Mater.* **2007**, *17*, 1636.
[24] V. Shrotriya, Y. Yao, G. Li, Y. Yang, *Appl. Phys. Lett.* **2006**, *89*, 063505.
[25] G. Li, V. Shrotriya, Y. Yao, J. S. Huang, Y. Yang, J.*Mater. Chem.* **2007**, *17*, 3126.
[26] F. L. Zhang, K. G. Jespersen, C. Bjorstrom, M. Svensson, M. R. Andersson, V. Sundstrom, K. Magnusson, E. Moons, A. Yartsev, O. Inganas, *Adv. Funct. Mater.* **2006**, *16*, 667.
[27] J. Peet, C. Soci, R. C. Coffin, T. Q. Nguyen, A. Mikhailovsky, D. Moses, G. C. Bazan, *Appl. Phys. Lett.* **2006**, *89*, 252105.
[28] F.-C. Chen, H.-C. Tseng, C.-J. Ko, *Appl. Phys. Lett.* **2008**, *92*, 103316.
[29] J. K. Lee, W. L. Ma, C. J. Brabec, J. Yuen, J. S. Moon, J. Y. Kim, K. Lee, G. C. Bazan, A. J. Heeger, *J. Am. Chem. Soc.* **2008**, *130*, 3619.
[30] A. J. Moulé, K. Meerholz, *Adv. Mater.* **2008**, *20*, 240.
[31] A. J. Moulé, K. Meerholz, *Adv. Funct. Mater.* **2009**, *19*, 3028.
[32] A. Swinnen, I. Haeldermans, M. vande Ven, J. D'Haen, G. Vanhoyland, S. Aresu, M. D'Olieslaeger, J. Manca, *Adv. Funct. Mater.* **2006**, *16*, 760.
[33] C. Müller, T. A. M. Ferenczi, M. Campoy-Quiles, J. M. Frost, D. D. C. Bradley, P. Smith, N. Stingelin-Stutzmann, J. Nelson, *Adv. Mater.* **2008**, *20*, 3510.
[34] B. Watts, W. J. Belcher, L. Thomsen, H. Ade, P. C. Dastoor, *Macromolecules* **2009**, *42*, 8392.
[35] T. A. Bull, L. S. C. Pingree, S. A. Jenekhe, D. S. Ginger, C. K. Luscombe, *ACS Nano* **2009**, *3*, 627.
[36] C. W. Frank, V. Rao, M. M. Despotopoulou, R. F. W. Pease, W. D. Hinsberg, R. D. Miller, J. F. Rabolt, *Science* **1996**, *273*, 912.
[37] I. Hadj Romdhane, P. E. Price, C. A. Miller, P. T. Benson, S. Wang, *Indust. Eng. Chem. Res.* **2001**, *40*, 3065.
[38] S. Bistac, J. Schultz, *Prog. Org. Coat.* **1997**, *31*, 347.
[39] J. García-Turiel, B. Jérôme, *Colloid Polymer Science* **2007**, *285*, 1617.
[40] H. Hansel, D. C. Muller, M. Gross, K. Meerholz, G. Krausch, *Macromolecules* **2003**, *36*, 4932.
[41] C. M. Bjorstrom, S. Nilsson, A. Bernasik, A. Budkowski, M. Andersson, K. O. Magnusson, E. Moons, *Appl. Surf. Sci.* **2007**, *253*, 3906.
[42] R. Osterbacka, C. P. An, X. M. Jiang, Z. V. Vardeny, *Science* **2000**, *287*, 839.
[43] Z. Y. Wu, A. Petzold, T. Henze, T. Thurn-Albrecht, R. H. Lohwasser, M. Sommer, M. Thelakkat, *Macromolecules* 2010, *43*,4646.
[44] M. T. Rispens, A. Meetsma, R. Rittberger, C. J. Brabec, N. S. Sariciftci, J. C. Hummelen, *Chem. Commun.* **2003**, 2116.
[45] Y. Kim, S. A. Choulis, J. Nelson, D. D. C. Bradley, S. Cook, J. R. Durrant, *Appl. Phys. Lett.* **2005**, *86*, 063502.